Search for $B \to K^*\nu\overline{\nu}$ decays

B. Aubert,[1] M. Bona,[1] Y. Karyotakis,[1] J. P. Lees,[1] V. Poireau,[1] E. Prencipe,[1] X. Prudent,[1] V. Tisserand,[1]
J. Garra Tico,[2] E. Grauges,[2] L. Lopez[ab],[3] A. Palano[ab],[3] M. Pappagallo[ab],[3] G. Eigen,[4] B. Stugu,[4] L. Sun,[4]
G. S. Abrams,[5] M. Battaglia,[5] D. N. Brown,[5] R. N. Cahn,[5] R. G. Jacobsen,[5] L. T. Kerth,[5] Yu. G. Kolomensky,[5]
G. Lynch,[5] I. L. Osipenkov,[5] M. T. Ronan,[5, *] K. Tackmann,[5] T. Tanabe,[5] C. M. Hawkes,[6] N. Soni,[6] A. T. Watson,[6]
H. Koch,[7] T. Schroeder,[7] D. Walker,[8] D. J. Asgeirsson,[9] B. G. Fulsom,[9] C. Hearty,[9] T. S. Mattison,[9]
J. A. McKenna,[9] M. Barrett,[10] A. Khan,[10] V. E. Blinov,[11] A. D. Bukin,[11] A. R. Buzykaev,[11] V. P. Druzhinin,[11]
V. B. Golubev,[11] A. P. Onuchin,[11] S. I. Serednyakov,[11] Yu. I. Skovpen,[11] E. P. Solodov,[11] K. Yu. Todyshev,[11]
M. Bondioli,[12] S. Curry,[12] I. Eschrich,[12] D. Kirkby,[12] A. J. Lankford,[12] P. Lund,[12] M. Mandelkern,[12]
E. C. Martin,[12] D. P. Stoker,[12] S. Abachi,[13] C. Buchanan,[13] J. W. Gary,[14] F. Liu,[14] O. Long,[14] B. C. Shen,[14, *]
G. M. Vitug,[14] Z. Yasin,[14] L. Zhang,[14] V. Sharma,[15] C. Campagnari,[16] T. M. Hong,[16] D. Kovalskyi,[16]
M. A. Mazur,[16] J. D. Richman,[16] T. W. Beck,[17] A. M. Eisner,[17] C. J. Flacco,[17] C. A. Heusch,[17] J. Kroseberg,[17]
W. S. Lockman,[17] A. J. Martinez,[17] T. Schalk,[17] B. A. Schumm,[17] A. Seiden,[17] M. G. Wilson,[17] L. O. Winstrom,[17]
C. H. Cheng,[18] D. A. Doll,[18] B. Echenard,[18] F. Fang,[18] D. G. Hitlin,[18] I. Narsky,[18] T. Piatenko,[18] F. C. Porter,[18]
R. Andreassen,[19] G. Mancinelli,[19] B. T. Meadows,[19] K. Mishra,[19] M. D. Sokoloff,[19] P. C. Bloom,[20]
W. T. Ford,[20] A. Gaz,[20] J. F. Hirschauer,[20] M. Nagel,[20] U. Nauenberg,[20] J. G. Smith,[20] K. A. Ulmer,[20]
S. R. Wagner,[20] R. Ayad,[21, †] A. Soffer,[21, ‡] W. H. Toki,[21] R. J. Wilson,[21] D. D. Altenburg,[22] E. Feltresi,[22]
A. Hauke,[22] H. Jasper,[22] M. Karbach,[22] J. Merkel,[22] A. Petzold,[22] B. Spaan,[22] K. Wacker,[22] M. J. Kobel,[23]
W. F. Mader,[23] R. Nogowski,[23] K. R. Schubert,[23] R. Schwierz,[23] A. Volk,[23] D. Bernard,[24] G. R. Bonneaud,[24]
E. Latour,[24] M. Verderi,[24] P. J. Clark,[25] S. Playfer,[25] J. E. Watson,[25] M. Andreotti[ab],[26] D. Bettoni[a],[26] C. Bozzi[a],[26]
R. Calabrese[ab],[26] A. Cecchi[ab],[26] G. Cibinetto[ab],[26] P. Franchini[ab],[26] E. Luppi[ab],[26] M. Negrini[ab],[26] A. Petrella[ab],[26]
L. Piemontese[a],[26] V. Santoro[ab],[26] R. Baldini-Ferroli,[27] A. Calcaterra,[27] R. de Sangro,[27] G. Finocchiaro,[27]
S. Pacetti,[27] P. Patteri,[27] I. M. Peruzzi,[27, §] M. Piccolo,[27] M. Rama,[27] A. Zallo,[27] A. Buzzo[a],[28] R. Contri[ab],[28]
M. Lo Vetere[ab],[28] M. M. Macri[a],[28] M. R. Monge[ab],[28] S. Passaggio[a],[28] C. Patrignani[ab],[28] E. Robutti[a],[28]
A. Santroni[ab],[28] S. Tosi[ab],[28] K. S. Chaisanguanthum,[29] M. Morii,[29] A. Adametz,[30] J. Marks,[30] S. Schenk,[30]
U. Uwer,[30] V. Klose,[31] H. M. Lacker,[31] D. J. Bard,[32] P. D. Dauncey,[32] J. A. Nash,[32] M. Tibbetts,[32] P. K. Behera,[33]
X. Chai,[33] M. J. Charles,[33] U. Mallik,[33] J. Cochran,[34] H. B. Crawley,[34] L. Dong,[34] W. T. Meyer,[34] S. Prell,[34]
E. I. Rosenberg,[34] A. E. Rubin,[34] Y. Y. Gao,[35] A. V. Gritsan,[35] Z. J. Guo,[35] C. K. Lae,[35] N. Arnaud,[36]
J. Béquilleux,[36] A. D'Orazio,[36] M. Davier,[36] J. Firmino da Costa,[36] G. Grosdidier,[36] A. Höcker,[36] V. Lepeltier,[36]
F. Le Diberder,[36] A. M. Lutz,[36] S. Pruvot,[36] P. Roudeau,[36] M. H. Schune,[36] J. Serrano,[36] V. Sordini,[36, ¶]
A. Stocchi,[36] G. Wormser,[36] D. J. Lange,[37] D. M. Wright,[37] I. Bingham,[38] J. P. Burke,[38] C. A. Chavez,[38]
J. R. Fry,[38] E. Gabathuler,[38] R. Gamet,[38] D. E. Hutchcroft,[38] D. J. Payne,[38] C. Touramanis,[38] A. J. Bevan,[39]
C. K. Clarke,[39] K. A. George,[39] F. Di Lodovico,[39] R. Sacco,[39] M. Sigamani,[39] G. Cowan,[40] H. U. Flaecher,[40]
D. A. Hopkins,[40] S. Paramesvaran,[40] F. Salvatore,[40] A. C. Wren,[40] D. N. Brown,[41] C. L. Davis,[41] A. G. Denig,[42]
M. Fritsch,[42] W. Gradl,[42] G. Schott,[42] K. E. Alwyn,[43] D. Bailey,[43] R. J. Barlow,[43] Y. M. Chia,[43] C. L. Edgar,[43]
G. Jackson,[43] G. D. Lafferty,[43] T. J. West,[43] J. I. Yi,[43] J. Anderson,[44] C. Chen,[44] A. Jawahery,[44] D. A. Roberts,[44]
G. Simi,[44] J. M. Tuggle,[44] C. Dallapiccola,[45] X. Li,[45] E. Salvati,[45] S. Saremi,[45] R. Cowan,[46] D. Dujmic,[46]
P. H. Fisher,[46] G. Sciolla,[46] M. Spitznagel,[46] F. Taylor,[46] R. K. Yamamoto,[46] M. Zhao,[46] P. M. Patel,[47]
S. H. Robertson,[47] A. Lazzaro[ab],[48] V. Lombardo[a],[48] F. Palombo[ab],[48] J. M. Bauer,[49] L. Cremaldi,[49]
R. Godang,[49, **] R. Kroeger,[49] D. A. Sanders,[49] D. J. Summers,[49] H. W. Zhao,[49] M. Simard,[50] P. Taras,[50]
F. B. Viaud,[50] H. Nicholson,[51] G. De Nardo[ab],[52] L. Lista[a],[52] D. Monorchio[ab],[52] G. Onorato[ab],[52] C. Sciacca[ab],[52]
G. Raven,[53] H. L. Snoek,[53] C. P. Jessop,[54] K. J. Knoepfel,[54] J. M. LoSecco,[54] W. F. Wang,[54] G. Benelli,[55]
L. A. Corwin,[55] K. Honscheid,[55] H. Kagan,[55] R. Kass,[55] J. P. Morris,[55] A. M. Rahimi,[55] J. J. Regensburger,[55]
S. J. Sekula,[55] Q. K. Wong,[55] N. L. Blount,[56] J. Brau,[56] R. Frey,[56] O. Igonkina,[56] J. A. Kolb,[56] M. Lu,[56]
R. Rahmat,[56] N. B. Sinev,[56] D. Strom,[56] J. Strube,[56] E. Torrence,[56] G. Castelli[ab],[57] N. Gagliardi[ab],[57]
M. Margoni[ab],[57] M. Morandin[a],[57] M. Posocco[a],[57] M. Rotondo[a],[57] F. Simonetto[ab],[57] R. Stroili[ab],[57] C. Voci[ab],[57]
P. del Amo Sanchez,[58] E. Ben-Haim,[58] H. Briand,[58] G. Calderini,[58] J. Chauveau,[58] P. David,[58] L. Del Buono,[58]
O. Hamon,[58] Ph. Leruste,[58] J. Ocariz,[58] A. Perez,[58] J. Prendki,[58] S. Sitt,[58] L. Gladney,[59] M. Biasini[ab],[60]

R. Covarelli[ab],[60] E. Manoni[ab],[60] C. Angelini[ab],[61] G. Batignani[ab],[61] S. Bettarini[ab],[61] M. Carpinelli[ab],[61, ††]
A. Cervelli[ab],[61] F. Forti[ab],[61] M. A. Giorgi[ab],[61] A. Lusiani[ac],[61] G. Marchiori[ab],[61] M. Morganti[ab],[61] N. Neri[ab],[61]
E. Paoloni[ab],[61] G. Rizzo[ab],[61] J. J. Walsh[a],[61] D. Lopes Pegna,[62] C. Lu,[62] J. Olsen,[62] A. J. S. Smith,[62]
A. V. Telnov,[62] F. Anulli[a],[63] E. Baracchini[ab],[63] G. Cavoto[a],[63] D. del Re[ab],[63] E. Di Marco[ab],[63] R. Faccini[ab],[63]
F. Ferrarotto[a],[63] F. Ferroni[ab],[63] M. Gaspero[ab],[63] P. D. Jackson[a],[63] L. Li Gioi[a],[63] M. A. Mazzoni[a],[63] S. Morganti[a],[63]
G. Piredda[a],[63] F. Polci[ab],[63] F. Renga[ab],[63] C. Voena[a],[63] M. Ebert,[64] T. Hartmann,[64] H. Schröder,[64] R. Waldi,[64]
T. Adye,[65] B. Franek,[65] E. O. Olaiya,[65] F. F. Wilson,[65] S. Emery,[66] M. Escalier,[66] L. Esteve,[66] S. F. Ganzhur,[66]
G. Hamel de Monchenault,[66] W. Kozanecki,[66] G. Vasseur,[66] Ch. Yèche,[66] M. Zito,[66] X. R. Chen,[67] H. Liu,[67]
W. Park,[67] M. V. Purohit,[67] R. M. White,[67] J. R. Wilson,[67] M. T. Allen,[68] D. Aston,[68] R. Bartoldus,[68]
P. Bechtle,[68] J. F. Benitez,[68] R. Cenci,[68] J. P. Coleman,[68] M. R. Convery,[68] J. C. Dingfelder,[68] J. Dorfan,[68]
G. P. Dubois-Felsmann,[68] W. Dunwoodie,[68] R. C. Field,[68] A. M. Gabareen,[68] S. J. Gowdy,[68] M. T. Graham,[68]
P. Grenier,[68] C. Hast,[68] W. R. Innes,[68] J. Kaminski,[68] M. H. Kelsey,[68] H. Kim,[68] P. Kim,[68] M. L. Kocian,[68]
D. W. G. S. Leith,[68] S. Li,[68] B. Lindquist,[68] S. Luitz,[68] V. Luth,[68] H. L. Lynch,[68] D. B. MacFarlane,[68]
H. Marsiske,[68] R. Messner,[68] D. R. Muller,[68] H. Neal,[68] S. Nelson,[68] C. P. O'Grady,[68] I. Ofte,[68] A. Perazzo,[68]
M. Perl,[68] B. N. Ratcliff,[68] A. Roodman,[68] A. A. Salnikov,[68] R. H. Schindler,[68] J. Schwiening,[68] A. Snyder,[68]
D. Su,[68] M. K. Sullivan,[68] K. Suzuki,[68] S. K. Swain,[68] J. M. Thompson,[68] J. Va'vra,[68] A. P. Wagner,[68]
M. Weaver,[68] C. A. West,[68] W. J. Wisniewski,[68] M. Wittgen,[68] D. H. Wright,[68] H. W. Wulsin,[68] A. K. Yarritu,[68]
K. Yi,[68] C. C. Young,[68] V. Ziegler,[68] P. R. Burchat,[69] A. J. Edwards,[69] S. A. Majewski,[69] T. S. Miyashita,[69]
B. A. Petersen,[69] L. Wilden,[69] S. Ahmed,[70] M. S. Alam,[70] J. A. Ernst,[70] B. Pan,[70] M. A. Saeed,[70] S. B. Zain,[70]
S. M. Spanier,[71] B. J. Wogsland,[71] R. Eckmann,[72] J. L. Ritchie,[72] A. M. Ruland,[72] C. J. Schilling,[72]
R. F. Schwitters,[72] B. W. Drummond,[73] J. M. Izen,[73] X. C. Lou,[73] F. Bianchi[ab],[74] D. Gamba[ab],[74] M. Pelliccioni[ab],[74]
M. Bomben[ab],[75] L. Bosisio[ab],[75] C. Cartaro[ab],[75] G. Della Ricca[ab],[75] L. Lanceri[ab],[75] L. Vitale[ab],[75] V. Azzolini,[76]
N. Lopez-March,[76] F. Martinez-Vidal,[76] D. A. Milanes,[76] A. Oyanguren,[76] J. Albert,[77] Sw. Banerjee,[77]
B. Bhuyan,[77] H. H. F. Choi,[77] K. Hamano,[77] R. Kowalewski,[77] M. J. Lewczuk,[77] I. M. Nugent,[77] J. M. Roney,[77]
R. J. Sobie,[77] T. J. Gershon,[78] P. F. Harrison,[78] J. Ilic,[78] T. E. Latham,[78] G. B. Mohanty,[78] H. R. Band,[79]
X. Chen,[79] S. Dasu,[79] K. T. Flood,[79] Y. Pan,[79] M. Pierini,[79] R. Prepost,[79] C. O. Vuosalo,[79] and S. L. Wu[79]

(The *BABAR* Collaboration)

[1]*Laboratoire de Physique des Particules, IN2P3/CNRS et Université de Savoie, F-74941 Annecy-Le-Vieux, France*
[2]*Universitat de Barcelona, Facultat de Fisica, Departament ECM, E-08028 Barcelona, Spain*
[3]*INFN Sezione di Bari[a]; Dipartimento di Fisica, Università di Bari[b], I-70126 Bari, Italy*
[4]*University of Bergen, Institute of Physics, N-5007 Bergen, Norway*
[5]*Lawrence Berkeley National Laboratory and University of California, Berkeley, California 94720, USA*
[6]*University of Birmingham, Birmingham, B15 2TT, United Kingdom*
[7]*Ruhr Universität Bochum, Institut für Experimentalphysik 1, D-44780 Bochum, Germany*
[8]*University of Bristol, Bristol BS8 1TL, United Kingdom*
[9]*University of British Columbia, Vancouver, British Columbia, Canada V6T 1Z1*
[10]*Brunel University, Uxbridge, Middlesex UB8 3PH, United Kingdom*
[11]*Budker Institute of Nuclear Physics, Novosibirsk 630090, Russia*
[12]*University of California at Irvine, Irvine, California 92697, USA*
[13]*University of California at Los Angeles, Los Angeles, California 90024, USA*
[14]*University of California at Riverside, Riverside, California 92521, USA*
[15]*University of California at San Diego, La Jolla, California 92093, USA*
[16]*University of California at Santa Barbara, Santa Barbara, California 93106, USA*
[17]*University of California at Santa Cruz, Institute for Particle Physics, Santa Cruz, California 95064, USA*
[18]*California Institute of Technology, Pasadena, California 91125, USA*
[19]*University of Cincinnati, Cincinnati, Ohio 45221, USA*
[20]*University of Colorado, Boulder, Colorado 80309, USA*
[21]*Colorado State University, Fort Collins, Colorado 80523, USA*
[22]*Technische Universität Dortmund, Fakultät Physik, D-44221 Dortmund, Germany*
[23]*Technische Universität Dresden, Institut für Kern- und Teilchenphysik, D-01062 Dresden, Germany*
[24]*Laboratoire Leprince-Ringuet, CNRS/IN2P3, Ecole Polytechnique, F-91128 Palaiseau, France*
[25]*University of Edinburgh, Edinburgh EH9 3JZ, United Kingdom*
[26]*INFN Sezione di Ferrara[a]; Dipartimento di Fisica, Università di Ferrara[b], I-44100 Ferrara, Italy*
[27]*INFN Laboratori Nazionali di Frascati, I-00044 Frascati, Italy*
[28]*INFN Sezione di Genova[a]; Dipartimento di Fisica, Università di Genova[b], I-16146 Genova, Italy*
[29]*Harvard University, Cambridge, Massachusetts 02138, USA*
[30]*Universität Heidelberg, Physikalisches Institut, Philosophenweg 12, D-69120 Heidelberg, Germany*
[31]*Humboldt-Universität zu Berlin, Institut für Physik, Newtonstr. 15, D-12489 Berlin, Germany*

[32]*Imperial College London, London, SW7 2AZ, United Kingdom*
[33]*University of Iowa, Iowa City, Iowa 52242, USA*
[34]*Iowa State University, Ames, Iowa 50011-3160, USA*
[35]*Johns Hopkins University, Baltimore, Maryland 21218, USA*
[36]*Laboratoire de l'Accélérateur Linéaire, IN2P3/CNRS et Université Paris-Sud 11,*
Centre Scientifique d'Orsay, B. P. 34, F-91898 Orsay Cedex, France
[37]*Lawrence Livermore National Laboratory, Livermore, California 94550, USA*
[38]*University of Liverpool, Liverpool L69 7ZE, United Kingdom*
[39]*Queen Mary, University of London, London, E1 4NS, United Kingdom*
[40]*University of London, Royal Holloway and Bedford New College, Egham, Surrey TW20 0EX, United Kingdom*
[41]*University of Louisville, Louisville, Kentucky 40292, USA*
[42]*Johannes Gutenberg-Universität Mainz, Institut für Kernphysik, D-55099 Mainz, Germany*
[43]*University of Manchester, Manchester M13 9PL, United Kingdom*
[44]*University of Maryland, College Park, Maryland 20742, USA*
[45]*University of Massachusetts, Amherst, Massachusetts 01003, USA*
[46]*Massachusetts Institute of Technology, Laboratory for Nuclear Science, Cambridge, Massachusetts 02139, USA*
[47]*McGill University, Montréal, Québec, Canada H3A 2T8*
[48]*INFN Sezione di Milano[a]; Dipartimento di Fisica, Università di Milano[b], I-20133 Milano, Italy*
[49]*University of Mississippi, University, Mississippi 38677, USA*
[50]*Université de Montréal, Physique des Particules, Montréal, Québec, Canada H3C 3J7*
[51]*Mount Holyoke College, South Hadley, Massachusetts 01075, USA*
[52]*INFN Sezione di Napoli[a]; Dipartimento di Scienze Fisiche,*
Università di Napoli Federico II[b], I-80126 Napoli, Italy
[53]*NIKHEF, National Institute for Nuclear Physics and High Energy Physics, NL-1009 DB Amsterdam, The Netherlands*
[54]*University of Notre Dame, Notre Dame, Indiana 46556, USA*
[55]*Ohio State University, Columbus, Ohio 43210, USA*
[56]*University of Oregon, Eugene, Oregon 97403, USA*
[57]*INFN Sezione di Padova[a]; Dipartimento di Fisica, Università di Padova[b], I-35131 Padova, Italy*
[58]*Laboratoire de Physique Nucléaire et de Hautes Energies,*
IN2P3/CNRS, Université Pierre et Marie Curie-Paris6,
Université Denis Diderot-Paris7, F-75252 Paris, France
[59]*University of Pennsylvania, Philadelphia, Pennsylvania 19104, USA*
[60]*INFN Sezione di Perugia[a]; Dipartimento di Fisica, Università di Perugia[b], I-06100 Perugia, Italy*
[61]*INFN Sezione di Pisa[a]; Dipartimento di Fisica,*
Università di Pisa[b]; Scuola Normale Superiore di Pisa[c], I-56127 Pisa, Italy
[62]*Princeton University, Princeton, New Jersey 08544, USA*
[63]*INFN Sezione di Roma[a]; Dipartimento di Fisica,*
Università di Roma La Sapienza[b], I-00185 Roma, Italy
[64]*Universität Rostock, D-18051 Rostock, Germany*
[65]*Rutherford Appleton Laboratory, Chilton, Didcot, Oxon, OX11 0QX, United Kingdom*
[66]*CEA, Irfu, SPP, Centre de Saclay, F-91191 Gif-sur-Yvette, France*
[67]*University of South Carolina, Columbia, South Carolina 29208, USA*
[68]*Stanford Linear Accelerator Center, Stanford, California 94309, USA*
[69]*Stanford University, Stanford, California 94305-4060, USA*
[70]*State University of New York, Albany, New York 12222, USA*
[71]*University of Tennessee, Knoxville, Tennessee 37996, USA*
[72]*University of Texas at Austin, Austin, Texas 78712, USA*
[73]*University of Texas at Dallas, Richardson, Texas 75083, USA*
[74]*INFN Sezione di Torino[a]; Dipartimento di Fisica Sperimentale, Università di Torino[b], I-10125 Torino, Italy*
[75]*INFN Sezione di Trieste[a]; Dipartimento di Fisica, Università di Trieste[b], I-34127 Trieste, Italy*
[76]*IFIC, Universitat de Valencia-CSIC, E-46071 Valencia, Spain*
[77]*University of Victoria, Victoria, British Columbia, Canada V8W 3P6*
[78]*Department of Physics, University of Warwick, Coventry CV4 7AL, United Kingdom*
[79]*University of Wisconsin, Madison, Wisconsin 53706, USA*
(Dated: November 3, 2008)

We present a search for the decays $B \to K^* \nu \overline{\nu}$ using 454×10^6 $B\overline{B}$ pairs collected at the $\Upsilon(4S)$ resonance with the BABAR detector at the SLAC PEP-II B-Factory. We first select an event sample where one B is reconstructed in a semileptonic or hadronic mode with one charmed meson. The remaining particles in the event are then examined to search for a $B \to K^* \nu \overline{\nu}$ decay. The charged K^* is reconstructed as $K^{*+} \to K^0_S \pi^+$ or $K^{*+} \to K^+ \pi^0$; the neutral K^* is identified in $K^{*0} \to K^+ \pi^-$ mode. We establish upper limits at 90% confidence level of $\mathcal{B}(B^+ \to K^{*+} \nu \overline{\nu}) < 8 \times 10^{-5}$, $\mathcal{B}(B^0 \to K^{*0} \nu \overline{\nu}) < 12 \times 10^{-5}$, and $\mathcal{B}(B \to K^* \nu \overline{\nu}) < 8 \times 10^{-5}$.

In the Standard Model (SM) the $b \to s\nu\overline{\nu}$ process occurs via one-loop box or electroweak penguin diagrams, as shown in Fig. 1, and it is therefore expected to be highly suppressed. Due to the absence of photon penguin contributions and long distance effects, the corresponding rate is predicted in the SM with smaller theoretical uncertainties than $b \to s\ell^+\ell^-$. In particular, the SM branching fraction for $B \to K^*\nu\overline{\nu}$ is expected to be $(1.3^{+0.4}_{-0.3}) \times 10^{-5}$ [1]. However, this could be enhanced in many new physics (NP) scenarios, where several mechanisms contribute to the rate. In Ref. [1] nonstandard Z^0 coupling contributions are computed, giving an enhancement of up to a factor 10. Moreover, new sources of missing energy, such as light dark matter candidates [2] or unparticles [3, 4], could contribute to the rate and produce a final state with a K^* [6] plus missing energy. The kinematics of the decay is described in terms of $s_{\nu\nu} = m^2_{\nu\nu}/m^2_B$, where $m_{\nu\nu}$ is the invariant mass of the neutrino pair and m_B is the B meson mass. NP effects can strongly affect the shape of the $s_{\nu\nu}$ distribution [1, 4], and this is taken into account in the present work to obtain a model independent limit.
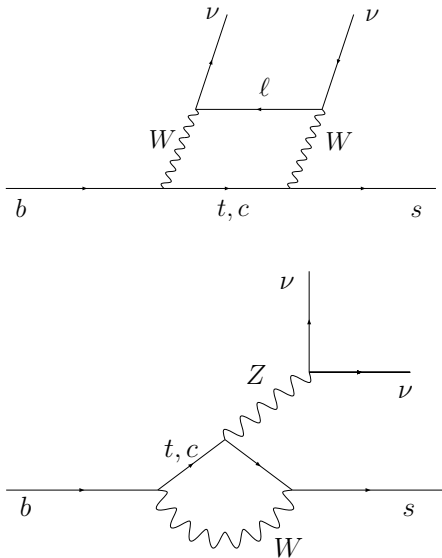

FIG. 1: SM diagrams for $b \to s\nu\overline{\nu}$ transitions.

*Deceased
†Now at Temple University, Philadelphia, Pennsylvania 19122, USA
‡Now at Tel Aviv University, Tel Aviv, 69978, Israel
§Also with Università di Perugia, Dipartimento di Fisica, Perugia, Italy
¶Also with Università di Roma La Sapienza, I-00185 Roma, Italy
**Now at University of South Alabama, Mobile, Alabama 36688, USA
††Also with Università di Sassari, Sassari, Italy

A previous search by the Belle Collaboration [5] sets upper limits of $\mathcal{B}(B^+ \to K^{*+}\nu\overline{\nu}) < 1.4 \times 10^{-4}$ and $\mathcal{B}(B^0 \to K^{*0}\nu\overline{\nu}) < 3.4 \times 10^{-4}$ at 90% confidence level [6].

In this paper we present the first BABAR search for both neutral and charged $B \to K^*\nu\overline{\nu}$ decays. The analysis is based on the data collected with the BABAR detector [7] at the PEP-II storage ring. The sample corresponds to an integrated luminosity of 413 fb^{-1} at the $\Upsilon(4S)$ resonance, consisting of about 454×10^6 $B\overline{B}$ pairs. An additional sample of 41 fb^{-1} was collected at a center of mass energy 40 MeV below the $\Upsilon(4S)$ resonance in order to study continuum events: $e^+e^- \to q\overline{q}$ ($q = u, d, s, c$) and $e^+e^- \to \tau^+\tau^-$. Charged-track reconstruction is provided by a silicon vertex detector and a drift chamber operating in a $1.5\,T$ magnetic field. Particle identification is based on the energy loss in the tracking system and the Cherenkov angle in an internally reflecting ring-imaging Cherenkov detector. Photon detection is provided by a CsI(Tl) electromagnetic calorimeter (EMC). Finally, muons are identified by the instrumented magnetic-flux return.

Pairs of photons with invariant mass between 115 and 150 MeV/c^2 are considered as π^0 candidates. The K^0_s candidates are reconstructed from pairs of oppositely charged pions.

A GEANT4-based [8] Monte Carlo (MC) simulation is used to model the detector response and test the analysis technique. Approximately 13×10^6 events are simulated where one B meson decays to a signal candidate mode and the other B decay is unconstrained (signal MC sample), and the kinematics of the signal decay is described by a pure phase space model. Simulated generic $B\overline{B}$ and continuum samples are used to investigate the background contamination and perform systematic studies.

Due to the presence of two undetected neutrinos in the final state, the $B \to K^*\nu\overline{\nu}$ decays cannot be fully reconstructed. Hence, one of the two B mesons produced in the $\Upsilon(4S)$ decay (the *tagging* B) is reconstructed in a semileptonic (B_{sl}) or a hadronic (B_{had}) mode containing a charmed meson. Then a K^* and missing energy are searched for in the rest of the event (ROE), defined as the set of tracks and EMC clusters not associated with the tagging B. The two tagging strategies provide non overlapping samples and the corresponding results can be combined as independent measurements. Selection criteria are applied to suppress the background contamination and an extended maximum likelihood fit is performed to extract the signal yields (N_s), which are finally used to determine the decay branching fractions ($\mathcal{B}$). In general, these can be written as:

$$\mathcal{B} = \frac{N_s}{\varepsilon \cdot N_{B\bar{B}}}, \tag{1}$$

where ε is the total signal efficiency measured with the signal MC sample and $N_{B\bar{B}}$ the number of produced $B\bar{B}$ pairs. In the semileptonic (SL) tagged analysis we

adopt Eq. (1) and use control samples to correct for small data/MC disagreements in the efficiency. In the hadronic (HAD) analysis, in order to avoid large systematic uncertainties associated with the MC estimate of the reconstruction efficiency for the B_had, we normalize the branching fraction with respect to the number of data events with a correctly reconstructed B_had (N_{B_had}):

$$\mathcal{B} = \frac{N_s}{\varepsilon_{B_\mathrm{sig}} \cdot N_{B_\mathrm{had}}} \cdot \frac{\varepsilon_{B_\mathrm{had}}^{B\overline{B}}}{\varepsilon_{B_\mathrm{had}}^{K^* \nu\overline{\nu}}}, \qquad (2)$$

where $\varepsilon_{B_\mathrm{sig}}$ is the efficiency related to the signal side reconstruction and selection, while $\varepsilon_{B_\mathrm{had}}^{B\overline{B}}$ and $\varepsilon_{B_\mathrm{had}}^{K^* \nu\overline{\nu}}$ are the B_had reconstruction efficiencies in events with generic $B\overline{B}$ decays and events containing the signal process, respectively; to account for differences among them, observed in the MC samples, their ratio $\varepsilon_{B_\mathrm{had}}^{K^* \nu\overline{\nu}}/\varepsilon_{B_\mathrm{had}}^{B\overline{B}}$ is used in Eq. 2 as a correction factor.

The event selection starts from the reconstruction of the tagging B. In the SL analysis, we search for a $B \to D^{(*)}l\nu$ decay. Neutral D mesons are reconstructed in the $K^-\pi^+$, $K^-\pi^+\pi^0$, $K^-\pi^+\pi^+\pi^-$ and $K_S^0\pi^+\pi^-$ modes. Charged D mesons are reconstructed in the $K^-\pi^+\pi^+$ and $K_S^0\pi^+$ final states. The D^{*0} candidates are reconstructed in the $D^{*0} \to D^0\gamma$ channel and the D^{*+} candidates in the $D^{*+} \to D^0\pi^+$ or $D^{*+} \to D^+\pi^0$ channels. Finally, a lepton (electron or muon) candidate is associated to the D meson and a kinematical fit is performed to find the B_sl decay vertex. Preliminary selection requirements are applied on the D mass (within 0.07 GeV/c^2 of the nominal mass in the $K^-\pi^+\pi^0$ mode, within 0.04 GeV/c^2 elsewhere) and the momentum of the lepton in the center of mass (CM) frame ($|\mathbf{p}_l^*| > 0.8$ GeV/c). We also require the CM angle between the B_sl and the $D^{(*)}l$ pair to satisfy $-5.0 < \cos\theta_{B,Dl} < 1.5$, where $\cos\theta_{B,Dl}$ can be calculated from the $D^{(*)}l$ four-momentum assuming that only one massless particle is missing:

$$\cos\theta_{B,Dl} = \frac{2E_{B,exp}^* E_{Dl}^* - m_B^2 - m_{Dl}^2}{2|\mathbf{p}_{B,exp}^*||\mathbf{p}_{Dl}^*|}. \qquad (3)$$

In Eq. 3, m_B is the nominal B mass, $E_{B,exp}^*$ and $|\mathbf{p}_{B,exp}^*|$ are the expected B energy and momentum, fixed by the energies of the beams and evaluated in the CM frame, and $|\mathbf{p}_{Dl}^*|$ is the $D^{(*)}l$ pair momentum in the CM frame. Values of $\cos\theta_{B,Dl}$ out of the physical range [-1,1] are due to resolution effects and missing particles in the Dl reconstruction. The distributions of the D mass and the lepton momentum in the CM frame, after the reconstruction of the signal B, are shown in Fig. 2. The plots are made after the signal reconstruction since in case of multiple B_sl candidates, the selection of the best one depends on the signal side reconstruction too, as will be discussed later; events where in the signal side a $K^{*+} \to K^+\pi^0$ channel is reconstructed are shown. If one $B \to D^{(*)}l\nu$ candidate can be reconstructed in the ROE with the same procedure adopted for the tag side, the event is selected as

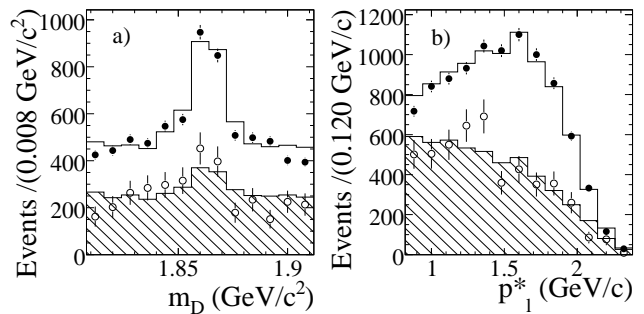a control sample of *double-tagged events* for systematic studies.

FIG. 2: The D mass a) and the CM momentum of the B_sl lepton b), in the SL analysis from MC simulations (histogram, the hatched area shows the continuum contribution), on-peak data ($\bullet$) and luminosity scaled off-peak data ($\circ$). Events where in the signal side a $K^{*+} \to K^+\pi^0$ channel is reconstructed are shown.

In the HAD analysis, we reconstruct B_had decays of the type $\overline{B} \to DY$, where D refers to a charm meson, and Y represents a collection of hadrons with a total charge of ± 1, composed of $n_1\pi^\pm + n_2 K^\pm + n_3 K_S^0 + n_4\pi^0$, where $n_1 + n_2 \leq 5$, $n_3 \leq 2$, and $n_4 \leq 2$. Using $D^0(D^+)$ and $D^{*0}(D^{*+})$ as seeds for $B^-(\overline{B}^0)$ decays, we reconstruct about 1000 different decay chains. Charmed mesons are reconstructed in the same final states used in the SL analysis, along with the additional channels $D^+ \to K^+\pi^+\pi^-\pi^0$, $K_S^0\pi^+\pi^+\pi^-$, $K_S^0\pi^+\pi^0$ and $D^{*0} \to D^0\pi^0$. B_had candidates are selected by the two kinematical variables:

$$\begin{aligned} m_\mathrm{ES} &= \sqrt{E_\mathrm{beam}^{*2} - |\mathbf{p}_B^*|^2} \\ \Delta E &= E_B^* - E_\mathrm{beam}^*, \end{aligned} \qquad (4)$$

where E_beam^* is the beam energy and E_B^* and $\mathbf{p}_B^*$ are the energy and the momentum of the B_had in the CM frame. For correctly tagged B candidates, the m_ES distribution peaks at the nominal B mass value and ΔE at zero. Hence, a selection is applied by requiring $-0.09 < \Delta E < 0.05$ GeV and $5.270 < m_\mathrm{ES} < 5.288$ GeV/c^2. The number of correctly reconstructed B_had events, to be used in Eq. (2), is extracted from the m_ES distribution of on-peak data. Background events are classified in four categories: combinatorial $B^0\overline{B}^0$, combinatorial B^+B^-, $e^+e^- \to c\overline{c}$ and $e^+e^- \to q\overline{q}$ ($q = u, d, s$). Other sources of background are found to be negligible. For each category, we extract the m_ES shape from MC simulations. The normalizations of the continuum contributions are taken from off-resonance data, scaled by the luminosity. The normalization of the $B\overline{B}$ contribution is extracted from a χ^2 fit in the $5.22 < m_\mathrm{ES} < 5.26$ GeV/c^2 region. The number of misreconstructed B_had in the signal region is extrapolated from the fit and subtracted from the data yield. In Fig. 3 the m_ES distributions for charged and neutral B_had are shown: the

on-peak data are superimposed to the estimated background contribution. After background subtraction, including correction factors and systematic uncertainties that will be discussed later, we determine $N_{B_{\mathrm{had}}} = (7.175 \pm 0.008(\mathrm{stat}) \pm 0.222(\mathrm{syst})) \times 10^5$ for neutral B_{had} and $N_{B_{\mathrm{had}}} = (10.128 \pm 0.010(\mathrm{stat}) \pm 0.344(\mathrm{syst})) \times 10^5$ for the charged B_{had}.
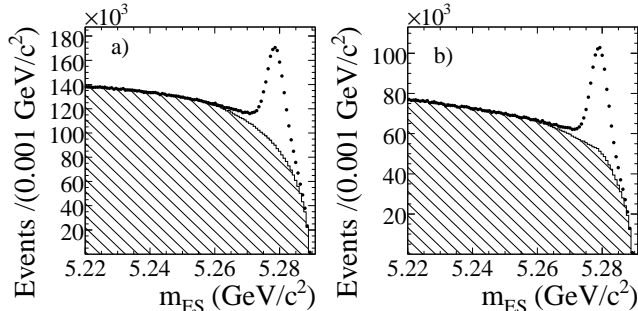
FIG. 3: The m_{ES} distributions for charged a) and neutral b) B_{had}. The points represent the on-peak data and the hatched area shows the estimated background contribution.

For each reconstructed tagging B, we search for a K^* candidate in the ROE. A neutral K^* can be reconstructed in the $K^+\pi^-$ mode, while a charged K^* can be reconstructed in the $K^0_S\pi^+$ and $K^+\pi^0$ channels. The number of tracks in the ROE is required to match exactly the number of expected tracks for the selected mode. The signal B must have opposite flavor (inferred from the K^* flavor) with respect to the tagging B.

If more than one $B_{\mathrm{sl}}(B_{\mathrm{had}}) - B_{\mathrm{sig}}$ pair has been reconstructed, only one of them is selected. In the SL analysis, we adopt a Bayesian approach to define the probability that both signal and tag side have been correctly reconstructed, given a set $\mathbf{x}$ of observed quantities:

$$P(TT|\mathbf{x}) = \frac{P(\mathbf{x}|TT)P(TT)}{\sum_i P(\mathbf{x}|i)P(i)} , \quad i = TT, TF, FT, FF \tag{5}$$

where TT (FF) indicates that both sides are correctly (wrongly) reconstructed and TF (FT) that only the tag (signal) side is correctly reconstructed. The candidate with the highest $P(TT|\mathbf{x})$ is retained. The set $\mathbf{x}$ is composed of the χ^2 probabilities of the B_{sl} and the K^* vertex fit. The corresponding likelihoods and prior probabilities are modeled from MC simulations with truth information to identify the correctly reconstructed candidates. In the HAD analysis, if more than one B_{had} is reconstructed, the best one is selected according to the smallest ΔE; if there are multiple K^* candidates associated to the best B_{had}, the one with a reconstructed mass closest to the world average value [9] is chosen.

Background contamination is reduced by applying a further selection on the $B\overline{B}$ candidates. Event shape variables, namely $\cos\theta^*_{B,\mathrm{T}}$ (the angle between the tag side reconstructed momentum and the thrust axis [10] of the ROE) and R_2 (the ratio of the second and zeroth Fox-Wolfram moments [11]), are used to reject the

TABLE I: Discriminating variables used in SL and HAD analyses and specific selection requirements. Values given in the squared brackets represent the lower and upper selection criteria imposed on the respective quantity.

Variable	Mode	Range	
		SL	HAD
$\cos\theta^*_{B,\mathrm{T}}$	$K^{*+} \to K^+\pi^0$	[-0.98,0.97]	
	$K^{*+} \to K^0_S\pi^+$	[-0.99,1.00]	[-0.95,0.95]
	$K^{*0} \to K^+\pi^-$	[-1.00,1.00]	
R_2	$K^{*+} \to K^+\pi^0$	[0.01,0.82]	
	$K^{*+} \to K^0_S\pi^+$	[0.01,0.71]	[0.00,0.70]
	$K^{*0} \to K^+\pi^-$	[0.00,0.80]	
m_{K^*}	$K^{*+} \to K^+\pi^0$	[0.83,0.97]	
(GeV/c^2)	$K^{*+} \to K^0_S\pi^+$	[0.85,0.95]	[0.84,0.96]
	$K^{*0} \to K^+\pi^-$	[0.84,0.97]	
$m_{K^0_S}$	$K^{*+} \to K^+\pi^0$	–	–
(GeV/c^2)	$K^{*+} \to K^0_S\pi^+$	[0.49,0.50]	[0.49,0.51]
	$K^{*0} \to K^+\pi^-$	–	–
$E^*_{\mathrm{miss}} + |\vec{p}^*_{\mathrm{miss}}|$	$K^{*+} \to K^+\pi^0$	[5.81,8.82]	
(GeV)	$K^{*+} \to K^0_S\pi^+$	[5.01,8.73]	–
	$K^{*0} \to K^+\pi^-$	[5.11,9.01]	
$\cos\theta^*_{\mathrm{miss}}$	$K^{*+} \to K^+\pi^0$	[-0.90,0.88]	
	$K^{*+} \to K^0_S\pi^+$	[-0.88,0.85]	[-0.90,0.90]
	$K^{*0} \to K^+\pi^-$	[-0.95,0.89]	
E_{extra}	$K^{*+} \to K^+\pi^0$		
(GeV)	$K^{*+} \to K^0_S\pi^+$	[0.00,1.20]	–
	$K^{*0} \to K^+\pi^-$		
$|\mathbf{p}^*_l|$	$K^{*+} \to K^+\pi^0$	[0.95,2.40]	
(GeV/c)	$K^{*+} \to K^0_S\pi^+$	[0.80,2.40]	–
	$K^{*0} \to K^+\pi^-$	[0.84,2.48]	

continuum background. The K^* mass (m_{K^*}) and, for the $K^0_S\pi^+$ mode, the K^0_S mass ($m_{K^0_S}$) allow rejection of combinatorial K^* candidates. We define the missing 4-momentum due to unreconstructed neutrinos as the difference between the $\Upsilon(4S)$ 4-momentum and the reconstructed tagging B and K^* 4-momenta. It is exploited in the selection through the combination $E^*_{\mathrm{miss}} + |\vec{p}^*_{\mathrm{miss}}|$ (the sum of the missing energy and the missing momentum evaluated in the CM frame) and the angle $\cos\theta^*_{\mathrm{miss}}$ (the azimuthal angle of the missing momentum in the CM frame). The extra neutral energy E_{extra}, defined as the sum of the energies of the EMC neutral clusters not used

TABLE II: Further selection requirements applied to the B_{sl} candidate (m_D^{PDG} is the nominal D mass [9]).

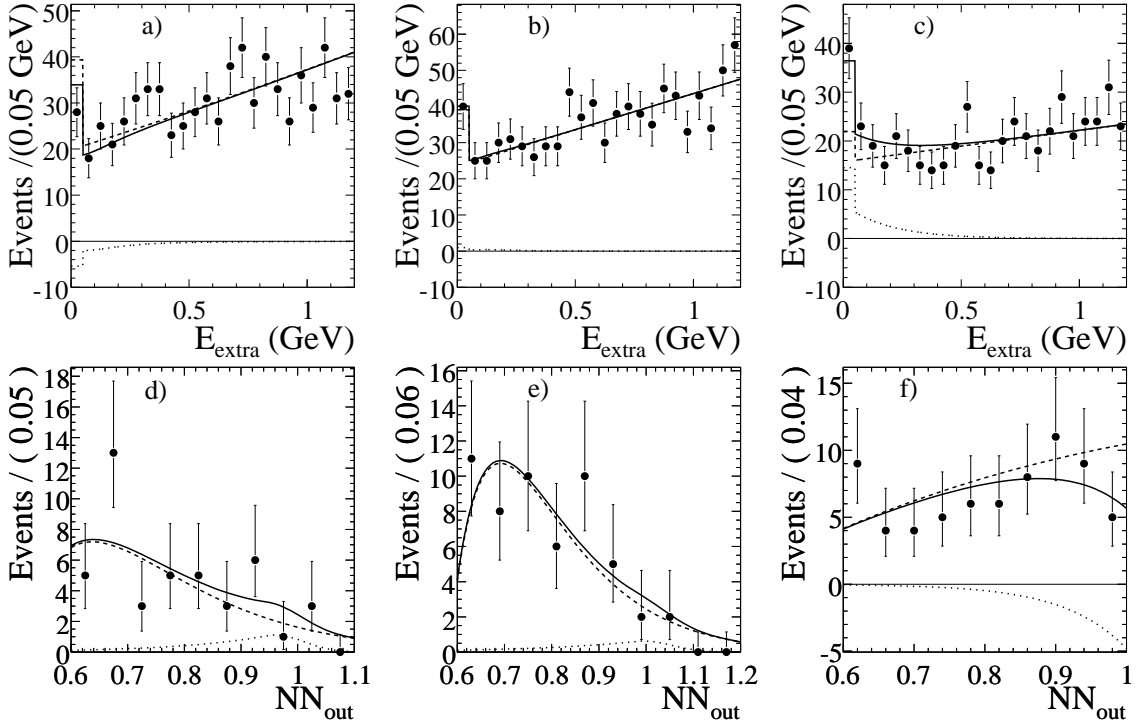| Variable	Mode	Range
$\cos\theta_{B,Dl}$	D^0 modes	[-2.00,1.00]
	$D^\pm$ modes	[-1.00,1.00]
$m_D - m_D^{PDG}$	$B^+ \to D^0(K^-\pi^+\pi^0)\ell^+\nu$	[-0.035,0.035]
(GeV/c^2)	other $B \to D\ell\nu$ modes	[-0.020,0.020]
Δm	$D^{*0} \to D^0\gamma$	[0.10,0.15]
(GeV/c^2)	$D^{*\pm} \to D^{\pm(0)}\pi^{0(\pm)}$	[0.14,0.15]

FIG. 4: Fit results for the extra EMC energy E_{extra} a) - c) for the SL analysis and the neural network output NN_{out} d) - f) for the HAD analysis. From left to right, $K^{*+} \to K^+ \pi^0$, $K^{*+} \to K^0_S \pi^+$ and $K^{*0} \to K^+ \pi^-$. Data are shown as points, and the fit result is shown with a solid line. The dotted and dashed lines show the estimated signal and background contributions respectively.

to reconstruct either the tag or the signal B, is exploited, considering that signal events have no additional neutral particles produced in association with the K^*. The requirements applied on the selection variables described above are listed in Tab. I.

In the SL analysis, the selection is optimized in the MC samples by maximizing the Punzi figure of merit [12], given by $\varepsilon/(n_\sigma/2 + \sqrt{N_b})$, where ε is the total signal efficiency, N_b is the number of expected background data events and $n_\sigma = 1.285$ corresponds to a one-side 90% confidence level. We also refine the B_{sl} selection with respect to the one applied before the choice of the best

candidate, and the corresponding requirements are summarized in Tab. II, where, Δm is the difference between the D and D^* masses, expected to be 142.17 ± 0.07 [9]. The total signal efficiency, evaluated with MC simulations, is given in Tab. III. The variable E_{extra} is not used in the selection optimization, and its distribution is used in an extended maximum likelihood fit in order to extract the signal yield. Due to the lower bound on the energy of detected photons (50 MeV), the distribution of E_{extra} is not continuous, so we define the likelihood in the following form:

$$
\begin{aligned}
\mathcal{L}(N_s, N_b) \;=\; & \frac{e^{-[(1-f_s)N_s + (1-f_b)N_b]}}{N_1!} \\
& \times \prod_{i=1}^{N_1} [P_{sig}(E_{extra,i}|\mathbf{p}_{sig})(1-f_s)N_s + P_{bkg}(E_{extra,i}|\mathbf{p}_{bkg})(1-f_b)N_b] \\
& \times \frac{(f_s N_s + f_b N_b)^{N_0} e^{-(f_s N_s + f_b N_b)}}{N_0!} \,,
\end{aligned}
\tag{6}
$$

where N_s and N_b are the expectation values for the numbers of signal and background events; f_s and f_b

TABLE III: Expected signal and background yields (N_s and N_b respectively) from MC studies (assuming the SM $\mathcal{B}$ for the signal) and results of the data fit, along with signal efficiencies, corrected for systematic effects. Expected signal yields are evaluated according to the SM expected $\mathcal{B}$. The first error on the fitted signal yield and on $N_{B_{\text{had}}}$ is statistical, the second is systematic. The corresponding upper limits are also quoted.

K^* mode	$K^+\pi^0$	$K_S^0\pi^+$	$K^+\pi^-$
		SL ANALYSIS	
Expected Yields			
N_s	3.31	2.54	4.07
N_b	697	827	468
E_{extra} Fit Results			
N_s	$-22 \pm 16 \pm 14$	$3 \pm 17 \pm 15$	$35 \pm 13 \pm 9$
N_b	754 ± 32	869 ± 34	476 ± 25
ε ($\times 10^{-4}$)	5.6 ± 0.7	4.3 ± 0.6	6.9 ± 0.8
$N_{B\bar{B}}$ ($\times 10^6$)		454 ± 5	
UL (90% CL)		9×10^{-5}	18×10^{-5}
		HAD ANALYSIS	
Expected Yields			
N_s	0.87	0.77	1.64
N_b	46	35	73
NN Fit Results			
N_s	$5 \pm 6 \pm 4$	$3 \pm 7 \pm 4$	$-10 \pm 9 \pm 6$
N_b	39 ± 9	51 ± 10	77 ± 13
$\varepsilon_{B_{\text{sig}}}$ ($\times 10^{-2}$)	5.8 ± 0.5	5.2 ± 0.6	16.6 ± 1.4
$N_{B_{\text{had}}}$ ($\times 10^5$)		$10.128 \pm 0.010 \pm 0.344$	$7.175 \pm 0.008 \pm 0.222$
UL (90% CL)		21×10^{-5}	11×10^{-5}

are the fractions of signal and background events with $E_{\text{extra}} = 0$, and are fixed from the results obtained in the MC samples; N_0 and N_1 are the numbers of observed events with $E_{\text{extra}} = 0$ and $E_{\text{extra}} > 50$ MeV respectively; and P_{sig} and P_{bkg} are the probability distribution functions (PDF) for signal and background, depending on a set of parameters $\mathbf{p}_{sig}$ and $\mathbf{p}_{bkg}$ respectively. MC studies show that the background distribution is well described by a first-order polynomial PDF, while the signal shape can be parameterized with an exponential function and, in the charged modes, with an additional Landau contribution that accounts for photons from a tag side D^* not associated to the B_{sl} during the reconstruction. The parameters of the PDFs are evaluated in the MC samples and fixed when fitting the real data. The fit strategy is validated by means of simulation studies which do not show any significant bias on the signal yields. The fits to the E_{extra} distributions in the data sample are shown in Fig. 4 and the fitted yields are quoted in Tab. III along with the total efficiencies ε.

In the HAD analysis, we apply a loose selection (Tab. I), then all discriminating variables are used as inputs for a Neural Network (NN), whose output variable NN_{out} is fitted in the region $NN_{\text{out}} > 0.6$, where the events from the signal MC sample are mostly concentrated. The upper bound of the fit region is different among the three K^* modes, reflecting the shape of NN_{out} in the signal MC sample. Three different NN are trained, one for each K^* decay mode. The signal output is described with an exponential function for the

$K^{*0} \rightarrow K^+\pi^-$ mode and a Crystal Ball PDF [13] for the charged K^* channels. The background is parameterized by

$$f(x) \propto \frac{x + k_1}{1 + e^{k_2 x}} . \tag{7}$$

Also in this case, in the fit to real data the signal and background PDF parameters are fixed to the values extracted from the MC simulations. Simulated experiments are used to validate the fit strategy. The fits to the NN_{out} distributions in the data sample are shown in Fig. 4, the fitted yields and the B_{sig} efficiencies $\varepsilon_{B_{\text{sig}}}$ are quoted in Tab. III.

The branching fraction measurement is affected by systematic uncertainties related to the signal efficiency estimate, the $\mathcal{B}$ normalization and the signal yield extraction from the fit.

The signal efficiency has an uncertainty due to the limited MC statistics. Control samples are used to estimate and correct for data/MC disagreement in the charged particle tracking, neutral particle reconstruction and particle identification. Uncertainties associated with the event selection criteria are computed depending on the specific selection strategy. Data/MC comparisons and expected detector resolutions provide an estimate of possible discrepancies in the distribution of the selection variables. For the SL analysis these values are used to vary the selection requirements and evaluate the impact on the efficiency; for the HAD analysis they are used to randomly smear the distributions of the NN inputs and

TABLE IV: Summary of systematic uncertainties on the signal efficiency, signal yield, and normalization.

K^* mode	SL ANALYSIS			HAD ANALYSIS		
	$K^+\pi^0$	$K_S^0\pi^+$	$K^+\pi^-$	$K^+\pi^0$	$K_S^0\pi^+$	$K^+\pi^-$
Signal efficiency (%)						
MC statistics	1.4	1.7	1.3	2.9	3.1	2.4
Best pair selection	0.2	0.0	0.0	–	–	–
Tagging Efficiency	10.0	10.0	10.0	–	–	–
Tracking	0.3	1.0	0.7	0.3	1.0	0.7
π^0 reconstruction	3.0	–	–	3.0	–	–
K_S^0 reconstruction	–	2.5	–	–	2.5	–
Particle ID	1.7	–	1.4	1.7	–	1.4
Selection variables	5.0	7.3	5.1	5.3	8.6	3.8
Model dependence	4.5	4.8	1.3	6.3	7.4	6.9
Signal yield (events)						
Signal PDF param.	0.7	1.4	0.2	0.2	0.3	0.2
Bkgd PDF param.	11.0	11.0	7.7	2.8	2.8	4.5
Signal PDF shape	–	–	–	1.2	1.7	1.2
Bkgd PDF shape	6.4	4.9	2.8	2.1	1.6	3.4
Normalization factor (%)						
N_{BB} or $N_{B_{\mathrm{had}}}$	1.1	1.1	1.1	3.4	3.4	3.1

evaluate the impact on the efficiency after the NN cut. The uncertainty due to the residual model dependence of our measurement is estimated as follows. We apply a weight to each MC event, based on the generated value of $s_{\nu\nu}$, in such a way that the weighted distribution matches the expected distribution in the SM or some specific NP model. Then the efficiency is evaluated taking into account the weights and is compared to the nominal efficiency (obtained from the unweighted MC events, generated with a pure phase space model). For the SL analysis two further uncertainties are associated with the best candidate selection and the B_{sl} selection efficiency. The former is evaluated by modifying the input likelihoods of Eq. (5) according to data/MC comparisons. Concerning the B_{sl} selection efficiency, we apply a correction given by the square root of the data/MC ratio of the number of double-tagged events. Alternative approaches are used to compute the same correction factor and the largest discrepancy with respect to the nominal approach is taken as a systematic uncertainty.

The error on the number of produced $B\overline{B}$ events is estimated as described in Ref [14]. The systematic error for $N_{B_{\mathrm{had}}}$, used in the HAD analysis, is computed by varying the MC $B\overline{B}$ component both in shape and normalization. The ratio $\varepsilon_{B_{\mathrm{had}}}^{K^* \nu\overline{\nu}}/\varepsilon_{B_{\mathrm{had}}}^{B\overline{B}}$, is used to correct the tag yield and to assign further systematic uncertainties. Since the tagging efficiency depends on the global event multiplicity, this ratio is expected to be different from 1 and to depend on the signal side decay and the B_{had} charge. From MC simulations it is found to be 1.008 ± 0.007 for the charged tag and 1.176 ± 0.013 for the neutral one.

The systematic uncertainties associated with the signal yield are due to the statistical errors on the PDF parameters (fixed from the MC sample) and potential data/MC disagreement for the shapes. We vary the parameters according to their statistical error and correlations. The background shapes are validated in the SL (HAD) analysis with the m_D (m_{ES}) sideband: the data/MC ratio of the fit variable distribution is parameterized by a first-order polynomial, that is used to modify the nominal background PDF. A similar strategy is adopted in the SL analysis to validate the signal PDF with double-tagged events. For the HAD analysis we compare the distributions of the NN output before and after the smearing of the inputs. In the SL analysis, also the statistical errors and the data/MC disagreements for the fractions f_s and f_b are included in these estimates. A summary of the systematic uncertainties is listed in Tab. IV.

No significant signal is observed in the two analyses. A Bayesian approach is used to set upper limits at the 90% confidence level on $\mathcal{B}_\pm = \mathcal{B}(B^+ \to K^{*+}\nu\overline{\nu})$, $\mathcal{B}_0 = \mathcal{B}(B^0 \to K^{*0}\nu\overline{\nu})$ and on their combination. Flat prior probabilities are assumed for positive values of both $\mathcal{B}$'s. Gaussian likelihoods are adopted for the observed signal yields, related to the $\mathcal{B}$'s by Eq. (1) or Eq. (2). The Gaussian widths are fixed to the sum in quadrature of the statistical and systematic yield errors. We extract a posterior two-dimensional PDF $P(\mathcal{B}_\pm, \mathcal{B}_0)$ using Bayes theorem, including in the calculation the effect of systematic uncertainties associated with the efficiencies and the normalizations, modeled by Gaussian PDFs. Systematic uncertainties that are common to the different channels and to the two analyses are assumed to be fully correlated. The 90% confidence level upper limits are calculated, after the marginalization of the two-dimensional posterior, by:

$$\int_0^{UL} \mathcal{P}_{0,\pm}(\mathcal{B}_{0,\pm}) \, d\mathcal{B}_{0,\pm} \bigg/ \int_0^\infty \mathcal{P}_{0,\pm}(\mathcal{B}_{0,\pm}) \, d\mathcal{B}_{0,\pm} = 0.9 \,. \tag{8}$$

The cross-feed between the different channels is found to be negligible in the MC events, but is included in the calculation for completeness. We extract the combined upper limits:

$$\mathcal{B}(B^+ \to K^{*+}\nu\overline{\nu}) < 8 \times 10^{-5}$$
$$\mathcal{B}(B^0 \to K^{*0}\nu\overline{\nu}) < 12 \times 10^{-5}$$
$$\mathcal{B}(B \to K^*\nu\overline{\nu}) < 8 \times 10^{-5}. \qquad (9)$$

In summary, we search for $B \to K^*\nu\overline{\nu}$ decays in a data sample corresponding to 413 fb^{-1}, collected by the BABAR experiment at the $\Upsilon(4S)$ resonance. We do not observe a significant signal in any of the modes studied and set upper limits on the decays $B^0 \to K^{*0}\nu\overline{\nu}$ and $B^+ \to K^{*+}\nu\overline{\nu}$, and the combined channel $B \to K^*\nu\overline{\nu}$. Since no constraints were applied to the kinematics of the final state K^* meson, or the undetected $\nu\overline{\nu}$ system, these results can be interpreted in the context of new physics models where invisible particles, other than neutrinos, are responsible for the missing energy [2–4]. In this way, the results presented here are model independent. These results represent the most stringent upper limits reported to date and they are still consistent with the SM expectation [1].

[1] G. Buchalla, G. Hiller and G. Isidori, Phys. Rev. D **63** (2001) 014015.

[2] C. Bird, P. Jackson, R. Kowalewski and M. Pospelov, Phys. Rev. Lett. **93** (2004) 201803.

[3] H. Georgi, Phys. Rev. Lett. **98** (2007) 221601.

[4] T. M. Aliev, A. S. Cornell and N. Gaur, JHEP **0707** (2007) 072

[5] K.-F. Chen *et al.* [BELLE Collaboration], Phys. Rev. Lett. **99** (2007) 221802.

[6] Charge conjugation is implied throughout this document, unless explicitly stated, and K^* refers to $K^*(892)$.

[7] B. Aubert *et al.* [BABAR Collaboration], Nucl. Instrum. Meth. A **479** (2002) 1.

[8] S. Agostinelli *et al.* [GEANT4 Collaboration], Nucl. Instrum. Meth. A **506** (2003) 250.

[9] W. M. Yao *et al.* [Particle Data Group], J. Phys. G **33** (2006) 1.

[10] S. Brandt, C. Peyrou, R. Sosnowski and A. Wroblewski, Phys. Lett. **12** (1964) 57; E. Farhi, Phys. Rev. Lett. **39** (1977) 1587.

[11] G. C. Fox and S. Wolfram, Phys. Rev. Lett. **41** (1978) 1581.

[12] G. Punzi, arXiv:physics/0308063.

[13] J. Gaiser *et al.*, Phys. Rev. D **34** (1986) 711.

[14] B. Aubert *et al.* [BABAR Collaboration], Phys. Rev. D **67**, (2003) 032002